

Compact lensless phase imager

MANON ROSTYKUS,^{1,*} FERRÉOL SOULEZ,² MICHAEL UNSER,² AND CHRISTOPHE MOSER¹

¹Ecole Polytechnique Fédérale de Lausanne, Laboratory of Applied Photonics Devices, CH-1015 Lausanne, Switzerland

²Ecole Polytechnique Fédérale de Lausanne, Biomedical Imaging Group, CH-1015 Lausanne, Switzerland

*manon.rostykus@epfl.ch

Abstract: Lensless quantitative phase imaging is of high interest for obtaining a large field of view (FOV), typically the size of the camera chip, to observe biological cell material with high contrast. It has the potential to be widely spread due to its inherent simplicity. However, the tradeoff is the added complexity due to the illumination. Current illumination systems are several centimeters away from the sample, use mechanics to obtain super resolution (i.e., smaller than the detector pixel size) or different illumination directions, and block the view to the sample. In this paper, we propose and demonstrate a side illumination system which reduces the height by an order of magnitude while providing an unobstructed view of the sample. We achieve this by shaping the illumination using multiplexed analog holograms that produce 9 illumination angles. We demonstrate experimentally imaging of phase samples with a FOV of $\sim 17\text{mm}^2$.

© 2017 Optical Society of America

OCIS codes: (050.1950) Diffraction gratings; (090.1995) Digital holography; (110.2945) Illumination design; (100.5070) Phase retrieval.

References

1. A. Greenbaum, W. Luo, T.-W. Su, Z. Göröcs, L. Xue, S. O. Isikman, A. F. Coskun, O. Mudanyali, and A. Ozcan, "Imaging without lenses: achievements and remaining challenges of wide-field on-chip microscopy," *Nat. Methods* **9**(9), 889–895 (2012).
2. S. Eisebitt, J. Lüning, W. F. Schlotter, M. Lörger, O. Hellwig, W. Eberhardt, and J. Stöhr, "Lensless imaging of magnetic nanostructures by X-ray spectro-holography," *Nature* **432**(7019), 885–888 (2004).
3. U. Schnars and W. Jueptner, *Digital Holography*. Berlin/Heidelberg: Springer-Verlag (2005).
4. O. Mudanyali, D. Tseng, C. Oh, S. O. Isikman, I. Sencan, W. Bishara, C. Oztoprak, S. Seo, B. Khademhosseini, and A. Ozcan, "Compact, light-weight and cost-effective microscope based on lensless incoherent holography for telemedicine applications," *Lab Chip* **10**(11), 1417–1428 (2010).
5. A. C. Sobieranski, F. Inci, H. C. Tekin, E. Comunello, A. Wangenheim, and U. Demirci, "Portable Digital in-Line Holography Platform for Sperm Cell Visualization and Quantification," 2014 27th SIBGRAPI Conf. Graph. Patterns Images, 274–281 (2014).
6. S. Seo, T.-W. Su, A. Erlinger, and A. Ozcan, "Multi-color LUCAS: Lensfree On-chip Cytometry Using Tunable Monochromatic Illumination and Digital Noise Reduction," *Cell. Mol. Bioeng.* **1**(2–3), 146–156 (2008).
7. A. Greenbaum, W. Luo, B. Khademhosseini, T.-W. Su, A. F. Coskun, and A. Ozcan, "Increased space-bandwidth product in pixel super-resolved lensfree on-chip microscopy," *Sci. Rep.* **3**, 1717 (2013).
8. W. Bishara, T.-W. Su, A. F. Coskun, and A. Ozcan, "Lensfree on-chip microscopy over a wide field-of-view using pixel super-resolution," *Opt. Express* **18**(11), 11181–11191 (2010).
9. D. Tseng, O. Mudanyali, C. Oztoprak, S. O. Isikman, I. Sencan, O. Yaglidere, and A. Ozcan, "Lensfree microscopy on a cellphone," *Lab Chip* **10**(14), 1787–1792 (2010).
10. S. Seo, T.-W. Su, D. K. Tseng, A. Erlinger, and A. Ozcan, "Lensfree holographic imaging for on-chip cytometry and diagnostics," *Lab Chip* **9**(6), 777–787 (2009).
11. K. Lee and Y. Park, "Quantitative phase imaging unit," *Opt. Lett.* **39**(12), 3630–3633 (2014).
12. A. S. G. Singh, A. Anand, R. A. Leitgeb, and B. Javidi, "Lateral shearing digital holographic imaging of small biological specimens," *Opt. Express* **20**(21), 23617–23622 (2012).
13. G. Liu and P. D. Scott, "Phase retrieval and twin-image elimination for in-line Fresnel holograms," *J. Opt. Soc. Am. A* **4**(1), 159 (1987).
14. B. M. Hennelly, D. P. Kelly, N. Pandey, and D. Monaghan, "Review of Twin Reduction and Twin Removal Techniques in Holography," in *Proceedings of the China-Ireland Information and Communications Technologies Conference*, National University of Ireland Maynooth, Ireland, (2009), pp. 241–245.
15. L. Denis, C. Fournier, T. Fournel, and C. Ducottet, "Twin-image noise reduction by phase retrieval in in-line

- digital holography,” in *Wavelets XI, SPIE’s Symposium on Optical Science and Technology* (2005), 59140J.
16. G. Koren, F. Polack, and D. Joyeux, “Iterative algorithms for twin-image elimination in in-line holography using finite-support constraints,” *J. Opt. Soc. Am. A* **10**(3), 423–433 (1993).
 17. C. Cho, B. Choi, H. Kang, and S. Lee, “Numerical twin image suppression by nonlinear segmentation mask in digital holography,” *Opt. Express* **20**(20), 22454–22464 (2012).
 18. G. Liu and P. D. Scott, “Phase retrieval and twin-image elimination for in-line Fresnel holograms,” *J. Opt. Soc. Am. A* **4**(1), 159 (1987).
 19. W. Luo, A. Greenbaum, Y. Zhang, and A. Ozcan, “Synthetic aperture-based on-chip microscopy,” *Light Sci. Appl.* **4**(3), e261 (2015).
 20. G. Zheng, R. Horstmeyer, and C. Yang, “Wide-field, high-resolution Fourier ptychographic microscopy,” *Nat. Photonics* **7**(9), 739–745 (2013).
 21. W. Bishara, U. Sikora, O. Mudanyali, T.-W. Su, O. Yaglidere, S. Luckhart, and A. Ozcan, “Holographic pixel super-resolution in portable lensless on-chip microscopy using a fiber-optic array,” *Lab Chip* **11**(7), 1276–1279 (2011).
 22. T.-W. Su, S. O. Isikman, W. Bishara, D. Tseng, A. Erlinger, and A. Ozcan, “Multi-angle lensless digital holography for depth resolved imaging on a chip,” *Opt. Express* **18**(9), 9690–9711 (2010).
 23. S. O. Isikman, W. Bishara, S. Mavandadi, F. W. Yu, S. Feng, R. Lau, and A. Ozcan, “Lens-free optical tomographic microscope with a large imaging volume on a chip,” *Proc. Natl. Acad. Sci. U.S.A.* **108**(18), 7296–7301 (2011).
 24. C. Zuo, J. Sun, J. Zhang, Y. Hu, and Q. Chen, “Lensless phase microscopy and diffraction tomography with multi-angle and multi-wavelength illuminations using a LED matrix,” *Opt. Express* **23**(11), 14314–14328 (2015).
 25. M. Guizar-Sicairos, S. T. Thurman, and J. R. Fienup, “Efficient subpixel image registration algorithms,” *Opt. Lett.* **33**(2), 156–158 (2008).
 26. F. Soulez, É. Thiébaud, A. Schutz, A. Ferrari, F. Courbin, and M. Unser, “Proximity operators for phase retrieval,” *Appl. Opt.* **55**(26), 7412–7421 (2016).
 27. A. Pu and D. Psaltis, “High-density recording in photopolymer-based holographic three-dimensional disks,” *Appl. Opt.* **35**(14), 2389–2398 (1996).
 28. G. Barbastathis, M. Levene, and D. Psaltis, “Shift multiplexing with spherical reference waves,” *Appl. Opt.* **35**(14), 2403–2417 (1996).
 29. E. Bostan, E. Froustey, M. Nilchian, D. Sage, and M. Unser, “Variational Phase Imaging Using the Transport-of-Intensity Equation,” *IEEE Trans. Image Process.* **25**(2), 807–817 (2016).
 30. Z. Jingshan, R. A. Claus, J. Dauwels, L. Tian, and L. Waller, “Transport of Intensity phase imaging by intensity spectrum fitting of exponentially spaced defocus planes,” *Opt. Express* **22**(9), 10661–10674 (2014).
 31. C. Edwards, B. Bhaduri, T. Nguyen, B. G. Griffin, H. Pham, T. Kim, G. Popescu, and L. L. Goddard, “Effects of spatial coherence in diffraction phase microscopy,” *Opt. Express* **22**(5), 5133–5146 (2014).
 32. G. Popescu, “Spatial light interference microscopy (SLIM),” *IEEE Photonic Soc. 24th Annu. Meet. PHO 2011*, **19**(2), 797 (2011).
 33. A. Pu and M. Spie, “Exposure schedule for multiplexing holograms in photopolymer films,” *Opt. Eng.* **35**, 2824–2829 (1996).

1. Introduction

Lensless imaging refers to an imaging technique which requires no imaging element between the light transmitted by the sample and the camera [1]. This configuration enables designing compact devices. It was initially developed for imaging in the X-ray and UV spectral ranges because of the difficulty to produce lenses in these ranges [2]. In the visible range, it is mainly investigated for microscopy, because lensless imaging provides, high resolution (sub-micrometer) with a large field of view equal to the size of the camera chip. Moreover, it also has the advantage to be cost effective since microscope objectives are expensive and bulky.

Digital inline holography has been investigated as a lensless interferometric technique, which requires only one illumination beam. The beam goes through the sample and part of the light is scattered by the elements of the size of the illumination. The other part of the light goes through unaffected. The scattered and unscattered fields are co-propagating and coherent with each other. They create an interferogram which is called an inline hologram on the camera. The images are then reconstructed numerically from the digital inline hologram [3]. This technique has been proposed with incoherent illumination [4–10] to create speckle free images; however, the compactness of the imager is then compromised since a rather large distance (several centimeters) is needed between the source and the sample to obtain enough spatial coherence. Other compact common-path interferometric methods have been investigated to obtain quantitative phase imaging based on lateral phase shifting [11,12].

In digital inline holography, the phase cannot be retrieved by only applying backpropagation to the recorded hologram. This is due to the fact that the real and virtual images are superimposed. This is known as “the twin image problem”. Several methods have been investigated to remove this twin image in order to be able to reconstruct the phase of the object along with its amplitude [13–18].

One of this phase retrieval technique uses a multi angle illumination [19,20]. During this process, several holograms are taken with different illumination directions. Then, the amplitude and the phase are numerically reconstructed using all those holograms. This technique has been proposed with an optical fiber mounted on a rotational arm [7,19] or several light-emitting diodes (LEDs) coupled in a fiber-optic array [21]. In this system, the distance between the end of the fiber and the object has to be quite large (several cm) to obtain enough spatial coherence. Moreover, the illumination is placed on top of the sample, which makes difficult additional measurements such as fluorescence imaging. This multi angle illumination can also be used to resolve depth in a volume [22–24].

In this paper, we present a lensless phase imager using a side illumination scheme that provides multiangle illumination of the sample. Digital inline holograms of purely phase objects are recorded on the imager for each illumination angle. In section 2, we present the side multi angle illumination in details. In section 3, we described the phase reconstruction. We present experimental results in section 4 and demonstrate intensity and phase reconstructions for a field of view of 17mm^2 and a device height of 10 mm.

2. Compact illumination

2.1 Multiplexed hologram gratings fabrication

The side illumination is fabricated with a K9 prism onto which a BAYFOL®HX photopolymer film of $70\mu\text{m}$ thickness from Covestro is laminated on one side, as shown in Fig. 1. The photopolymer has a similar refractive index as the prism and is used to record several analogic hologram gratings to obtain a multi angle illumination system.

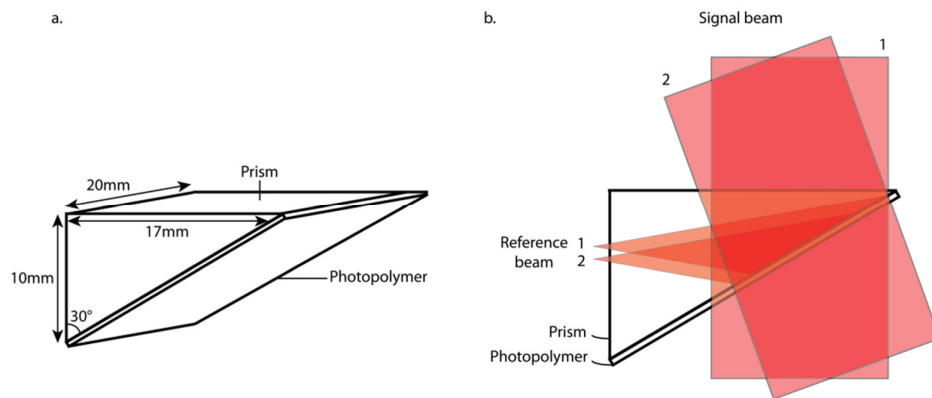


Fig. 1. (a) 3D sketch of the prism with a laminated photopolymer film. (b) Side view showing multiplexing of two hologram gratings. Reference beam 1 and signal beam 1 interfere in the photopolymer film inducing index of refraction changes, which result in a phase volume grating. Then the prism is moved to have the reference beam at position 2 and the signal beam direction is changed to obtain angle 2. The two beams interfere in the photopolymer inducing another phase hologram grating.

In order to record the hologram gratings, an interferometric setup is used. A continuous-wave, single frequency red laser (681nm Ondax Compact module) is collimated and split by a beam splitter to generate a plane signal beam and a spherical reference beam. The reference and the signal beams interfere in the photopolymer and induce a change of refractive index, which results in a phase volume grating. The wavefront of the reference beam is chosen to be

similar to the wavefront of a vertical cavity surface emitting laser (VCSEL). AVCSEL is used as the illumination source in the imager.

In order to obtain several illumination directions, the recording process is sequentially repeated, with each time a different position for the reference beam and a different angle for the signal beam, as shown in Fig. 1(b). Several hologram gratings are consequently angularly multiplexed in the photopolymer. The angle of the signal beam with respect to the normal to the prism is controlled with a 2D galvo mirror system (not shown) (Thorlabs GVS) and the position of the reference beam along the entrance surface of the prism is controlled by a translation stage (Newport CONEX-CC).

After recording, the photopolymer is cured using white light at $\sim 1.8\text{W}$ during $\sim 2\text{min}$.

2.2 Side illumination with VCSELs

Single mode VCSELs are used as readout sources of the hologram gratings. VCSELs are low power consumption lasers ($\sim 1\text{mW}$) which make them suitable for battery operation. It is envisioned that an array of VCSELs can be placed as illustrated in Fig. 2.

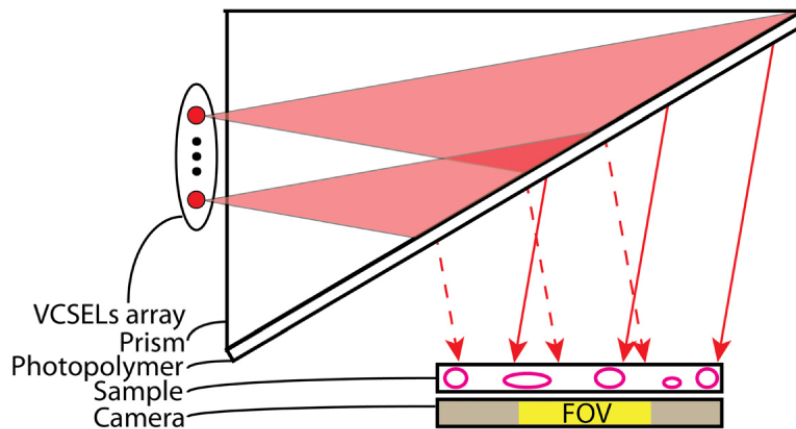


Fig. 2. 2D sketch of the compact phase imager with a side illumination system composed of VCSELs illuminating the multiplexed hologram on a photopolymer (fabricated according to Fig. 1 (b)). For clarity only two angles of illumination out of 9, corresponding to two VCSELs, are shown. All the beams overlap on a $\sim 17\text{mm}^2$ FOV, corresponding to $\sim 50\%$ of the camera chip size.

Each VCSEL position is determined by the focus point of the reference beam used during the recording process of the gratings. For each VCSEL, one diffracted beam will illuminate the sample with one illumination direction. The zero order beam (i.e. the through undiffracted beam) from the VCSELs are reflected by the prism by Total Internal Reflection and exit via the top facet of the prism. This is important because the zero order beam would create otherwise a strong background noise.

All the beams overlap on a $\sim 17\text{mm}^2$ FOV, corresponding to $\sim 50\%$ of the camera chip size. This is a current limitation that can be overcome by adding a lenslet array in front of the VCSELs to increase the numerical aperture of the sources.

3. Reconstruction algorithm

For each illumination direction, the hologram of the sample is shifted on the camera by an amount corresponding to the illumination angle. Shifts of all the holograms are estimated [25] using the hologram taken with normal incidence as reference. Knowing the distance sample-camera, each illumination angles (ϕ, θ) in 2D is determined as

$$\varphi = \arctan\left(\frac{x \cdot p}{z}\right), \quad \theta = \arctan\left(\frac{y \cdot p}{z}\right)$$

where x (resp. y) is the shift in pixel in the x direction (resp. y) of the hologram on the camera plane; p is the pixel size and z is the distance sample-camera.

The 9 inline digital holograms are then used in an amplitude and phase retrieval algorithm.

To recover the phase of the sample from the stack of inline holograms taken with different illumination directions, we used an “inverse problem” approach. A tilted illumination of the sample induces a shift of its Fourier transform. To fully exploit the information content of these measurements, the sample is reconstructed on a finer grid (up sampled by a factor 4 in the presented experiments). Our algorithm iteratively estimates the solution that fits the measurements while enforcing some prior knowledges (smoothness and unit modulus) by means of a suitable proximity operator [26].

The beam homogeneity is affected by the shrinkage induced by the curing [27], corresponding to a reduction of the photopolymer thickness of 3%. To tackle this issue, the algorithm utilizes intensity background images (i.e. without sample) as a calibration step to correct for this inhomogeneity.

A precise description of this algorithm is outside of the scope of this paper and its complete characterization will be described elsewhere.

4. Experimental results and discussion

4.1 Multiplexing

Cross talk is the effect of having several diffracted beams corresponding to a single reference source. This effect needs to be minimized in order to avoid artifacts in the reconstruction. To experimentally quantify cross talk, the shift selectivity is measured. Figure 3(a) shows the diffraction efficiency of a single phase grating with respect to the in-plane position of the readout point source along the entrance surface of the prism. The peak width gives the shift selectivity. The simulation is based on [28] including the prism geometry. The deviation between the simulation and the measurement comes from the effective thickness of the recorded phase grating, which is smaller than the physical film thickness of $70\mu\text{m}$. The corresponding effective thickness is $45\mu\text{m}$.

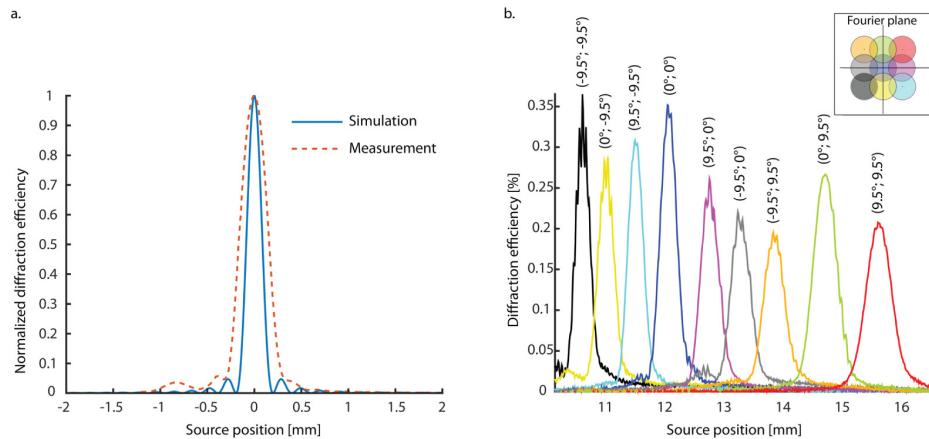


Fig. 3. (a) Normalized diffraction efficiency versus source position ($\varphi = -11.5^\circ$, $\theta = -11.5^\circ$). The experimental curve is broader than what is expected by the theory. The deviation between the simulation and the measurement come from the effective thickness of photopolymer used to record the grating, which is smaller than the expected $70\mu\text{m}$. (b) Diffraction efficiencies of 9 multiplexed hologram gratings versus source position along the entrance surface of the prism.

Figure 3(b) represents the diffraction efficiency curves of 9 multiplexed holograms with respect to the in-plane source position along the entrance surface of the prism using the same laser source for recording and readout. To obtain these curves, the prism was installed on a translation stage which was moved in front of the laser source.

We observe that the main contribution of the cross talk comes from the beam corresponding to adjacent point sources. In the worst case the relative crosstalk is less than 6% of the main peak, which was found acceptable for the reconstruction algorithm. This is important to avoid having different digital holograms recorded at the same time, which will result in an overlay of holograms. The efficiency of each peak is quite low which can be explained by the fact that the two recording beams on the photopolymer were not exactly of the same size. Consequently the hologram is smaller than the reference beam.

4.2 Phase recovery

The prism with the hologram gratings was then placed in front of a VCSEL (Vixar 680S) with a wavelength of 673nm and a linewidth of 100MHz on a translation stage. A single VCSEL is used as read out source of the hologram gratings for experimental convenience. The source is aligned with a 6 axis stage to maximize diffraction efficiency of one hologram. By construction, all other gratings are then automatically aligned when the VCSEL is translated. Each position of the VCSEL corresponds to one diffracted beam with a specific illumination direction. A digital hologram is recorded for each 9 positions. The camera (Thorlabs DCC1545M) pixel size is 5.2 μm and the field of view (FOV) is $\sim 17\text{mm}^2$.

First, 9 digital holograms of a custom made 1951 USAF phase test target were recorded. The reconstructed amplitude and phase are shown in Fig. 4. A comparison between the phase reconstructed with the proposed device and a phase image obtained with a digital holographic microscope (DHM) using a 5X objective is shown in Fig. 4. The depth measured in the reconstructed phase with the proposed technique and DHM is $\sim 215\text{nm}$ showing that the phase recovery method is accurate with 9 angles. Halos and poor estimations of large flat regions (see full FOV in Fig. 4(a)) are due to a noisy estimation of low frequencies phase. Indeed, inline holograms of phase objects cannot capture low frequency phase information. This effect is also present in transport of intensity experiments that share similar experimental conditions (i.e. sample-camera distance $< 900\mu\text{m}$) [29,30] and other quantitative phase imaging techniques [31,32]. However, lensless phase imagers are mainly used to image biological samples like cells [4–10] which sizes are typically less than $20\mu\text{m}$ for which the phase can be correctly computed.

The resolution obtained with the imager is $6.2\mu\text{m}$ (limited by the imager pixel size) over a FOV of $\sim 17\text{mm}^2$. Note that the DHM has a much smaller FOV ($\sim 4\text{mm}^2$) for a resolution of $\sim 4\mu\text{m}$.

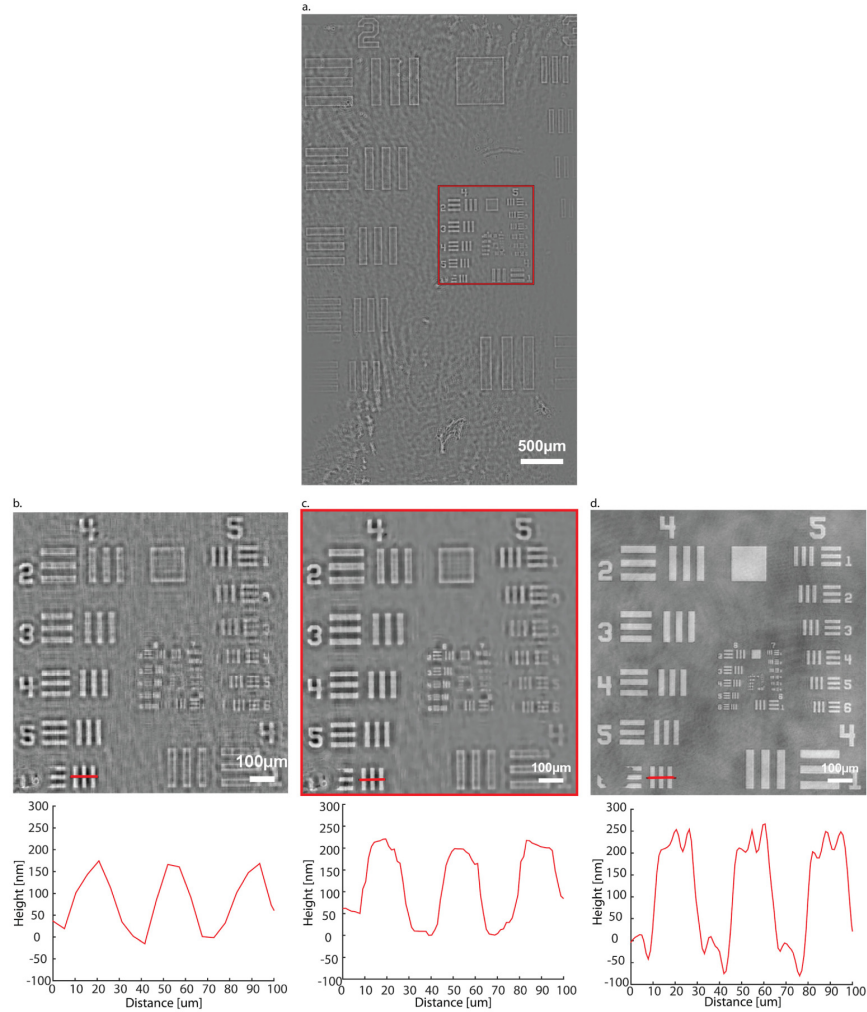


Fig. 4. (a) Reconstructed phase with the proposed device and algorithm of the full FOV. Halos in the large flat regions are due to a noisy estimation of low frequencies phase. This effect is also present in transport of intensity experiments and other quantitative phase imaging techniques (b) Reconstructed phase using only one hologram backpropagated with the angular spectrum method (crop of 1.1x1.1mm). (c) Reconstructed phase with the proposed device and algorithm (crop of 1.1x1.1mm). (d) Reconstructed phase with a Digital Holographic Microscope (DHM) (crop of 1.1x1.1mm).

The nine source positions cover a distance of 5.5mm of the prism height. Consequently, more analogic hologram gratings could be recorded (~18 in height along the in-plane direction and approximately the same amount in the out of plane direction) to increase the information redundancy for the algorithm. The efficiency of each hologram decreases with M^2 (with M the number of holograms) [33]. Each VCSEL provides ~1mW optical power, so 2.5μW illuminates the sample per angle for each of the 9 beam directions. With this power, an exposure time of 0.45ms is necessary to record a digital hologram, so in total 4ms would be necessary to record 9 digital holograms. Depending on the application this can allow quasi-live recording.

5. Conclusion

In this paper, we presented a lensless compact phase imager. A side illumination combining VCSELs, a prism and hologram gratings was developed to obtain a 10mm height imaging device, which is almost one order of magnitude shorter than other lensless imagers of comparable FOV. A new phase retrieval algorithm was also implemented allowing the reconstruction of the phase from 9 in-line digital holograms.

To demonstrate the phase retrieval ability of the presented device, digital holograms of a 1951 USAF phase test target were recorded. The 9 digital holograms were recorded with 9 different illumination directions obtained by illuminating the device using a VCSEL at 673nm as a readout source for the analogic hologram gratings. A phase image of the target was recovered. To verify that the retrieved phase is quantitative, control phase images from a DHM were taken. The computed heights were similar in both situations, proving the ability of the presented imager to do quantitative phase retrieval.

The imager has a free visual access to the sample from the top which allow for different imaging modalities at the same time, for example fluorescence imaging with a standard widefield microscope. Further work on improving the resolution and the building of a stand-alone version with a VCSELs array is ongoing.

Funding

European Research Council (grant No 692726 “GlobalBioIm: Global integrative framework for Computational Bio-Imaging”).

Acknowledgments

The authors would like to acknowledge Mathieu Künzi for the images from DHM and Enrico Chinello for providing the 1951 USAF phase test target.